

## Nanoscale live-cell imaging using hopping probe ion conductance microscopy

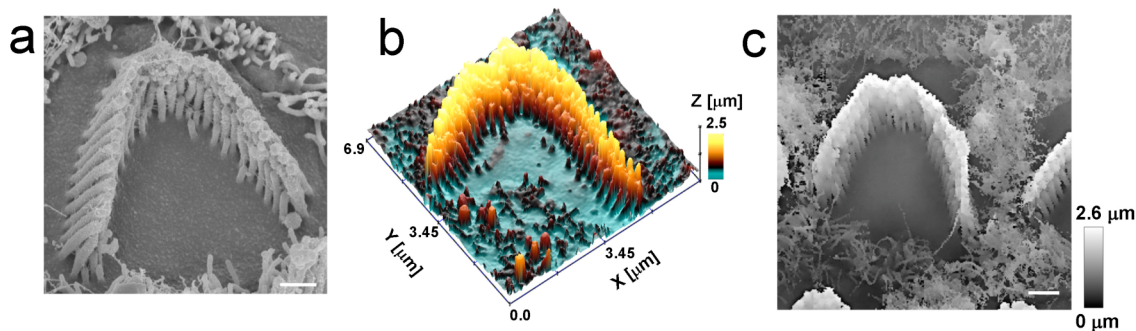
Pavel Novak, Chao Li, Andrew I Shevchuk, Ruben Stepanyan, Matthew Caldwell, Simon Hughes, Trevor G Smart, Julia Gorelik, Victor P Ostanin, Max J Lab, Guy W J Moss, Gregory I Frolenkov, David Klenerman & Yuri E Korchev

Supplementary figures and text:

<b>Supplementary Figure 1</b>	<b>Visualisation of vertically protruding mechanosensitive stereocilia of wild type outer hair cells: HPICM and SEM comparison.</b>
<b>Supplementary Figure 2</b>	<b>HPICM images of live hippocampus neuron cells.</b>
<b>Supplementary Figure 3</b>	<b>Visualisation of possible synaptic boutons by HPICM and confocal microscopy.</b>
<b>Supplementary Methods</b>	

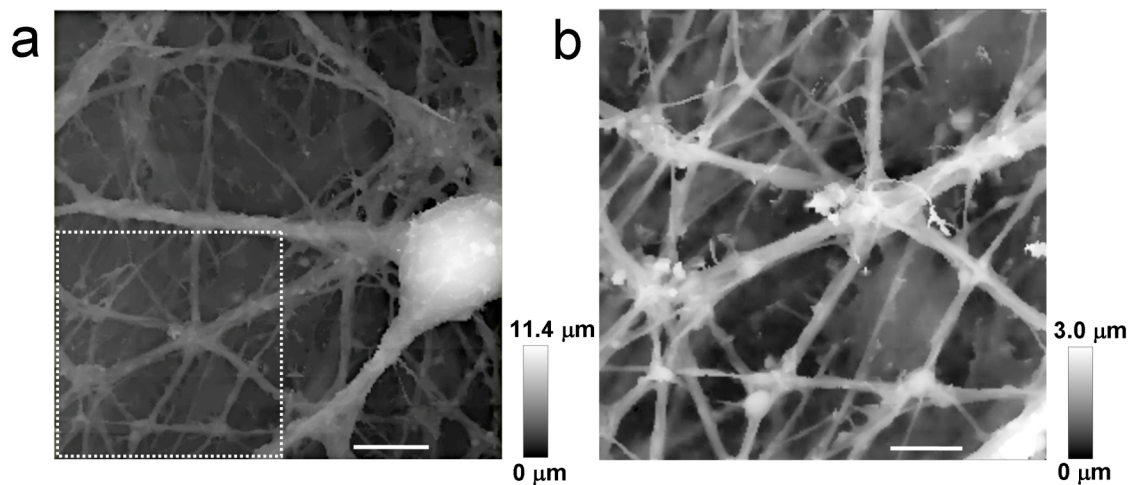
**Supplementary Figure 1.**

**Visualisation of vertically protruding mechanosensitive stereocilia of wild type outer hair cells: HPICM and SEM comparison.**



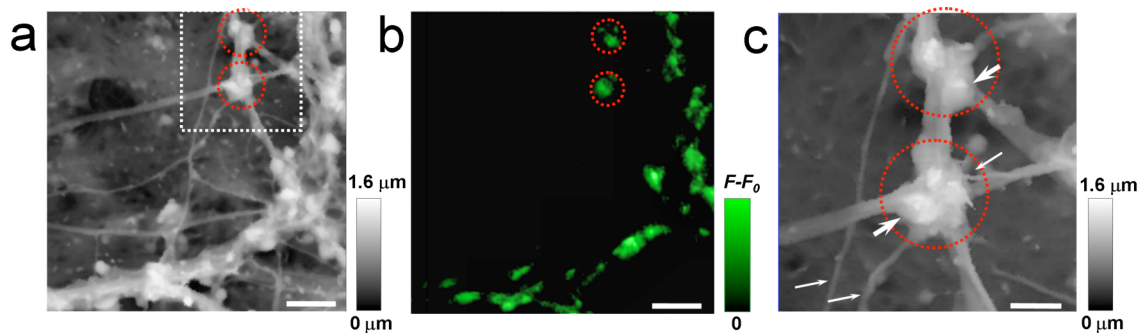
Images of the fixed specimens of the cultured mouse organs of Corti were obtained by SEM (a) and by HPICM (b,c). Note that HPICM is capable of producing clear images of hair bundles and surrounding microvilli even when the specimen has some debris that was left after detaching the overlying tectorial membrane (c). All the hair cells were approximately at the middle of the cochlea. In the HPICM images, the height of the sample is indicated by colour (b) or grey scale (c). Scale bars: a 500 nm; c 1 μm.

**Supplementary Figure 2.**  
HPICM images of live hippocampal neuron cells.



Panel **a** shows an image of a large area of the neural network. Panel **b** is a zoom of the dotted region in **a**. Scale bars: **a** 10 m; **b** 5 m.

**Supplementary Figure 3.**  
**Visualisation of possible synaptic boutons by HPICM and confocal microscopy.**



HPICM (**a**) and fluorescent (**b**) images of live hippocampal neuron cells with several possible synaptic boutons. The neurons were stained with a live marker of synaptic activity, FM1-43. (**c**) A high resolution image of the region in the top right corner of **a**. Potential synaptic boutons are marked with large arrows. Fine processes, probably axons, are marked by thin arrows. Scale bars: **a & b** 5 m; **c** 2 m.

## Supplementary Methods

### Solutions

The standard external solution used for imaging of hippocampal neurons contained (mM): NaCl 145; KCl 3; CaCl<sub>2</sub> 2.5; MgCl<sub>2</sub> 1.2; Glucose 10; HEPES 10. The loading solution used for FM1-43 staining of synaptic boutons contained (mM): NaCl 103; KCl 45; CaCl<sub>2</sub> 2.5; MgCl<sub>2</sub> 1.2; Glucose 10; HEPES 10 and 10 μM FM1-43 (Molecular Probes). PBS (composition, in mM, NaCl 137, KCl 2.7, KH<sub>2</sub>PO<sub>4</sub> 1.5, Na<sub>2</sub>HPO<sub>4</sub> 4.3, pH 7.2) was used as external solution for high resolution imaging of the fixed cultured organ of Corti explants. Nanopipettes were filled with PBS in all experiments. Both the external and pipette solutions were filtered using sterile 0.2 μm Acrodisc Syringe Filters (Pall Corporation, USA) to minimize blockage of nanopipettes during imaging.

### Cultured organs of Corti

Mice were derived from a colony reported previously<sup>1</sup>. Organ of Corti explants were dissected at postnatal days 2-4 (P2-4) and placed in glass-bottom Petri dishes (WillCo Wells, Netherlands). The explants were cultured in DMEM medium supplemented with 25 mM HEPES and 7% fetal bovine serum (Invitrogen, Carlsbad, CA) at 37°C and 95% air / 5% CO<sub>2</sub>. Cultured organs of Corti were used in experiments within 1-5 days. In some experiments, 10 g/ml of ampicillin (Calbiochem, La Jolla, CA) was added to the medium. The organs of Corti from left and right cochleae of a mouse were processed simultaneously. The cultured organs of Corti were immersed in 2.5% glutaraldehyde in 0.1M cacodylate buffer supplemented with 2 mM CaCl<sub>2</sub> for 1-2 hours at room temperature. One cochlea was used for HPICM imaging while the other one was used for SEM imaging. All animal procedures were approved by the University of Kentucky Animal Care and Use Committee.

### Hippocampal neurons preparation

Rat hippocampal neurons were prepared as previously described<sup>2</sup> and cultured on glass coverslips to allow confocal microscopy. Cells were kept in an incubator at 37 °C and 95% air / 5 % CO<sub>2</sub> for 1 to 2 weeks. Once out of the incubator, cells were washed with standard external solution and imaged within two hours, at room temperature. For combined topography/fluorescent measurements hippocampal neurons were first incubated for 90 seconds at room temperature in 1.5 ml of loading solution to stain synaptic boutons with FM1-43, an activity-dependent marker that is accumulated in synaptic vesicles during cycles of endo- and exocytosis<sup>3,4</sup>, and then washed three times with a total volume of at least 10 ml of standard external solution and left for 15 min in the dark before imaging. All animal procedures were done in compliance with Home Office (UK) regulations and Animals (Scientific Procedures) Act, 1986 and approved by local animal ethics committee of University College London.

### HPICM probes

Nanopipettes were pulled from borosilicate glass (O.D. 1 mm, I.D. 0.58, Intracell, UK) using a laser-based puller Model P-2000 (Sutter Instruments Co., USA). Two different pipettes were used: Standard pipettes, displayed resistances ranging from 100 M to 150 M (measured in a standard external solution) and inner diameter of 100 nm. These pipettes were used for scanning hippocampal neurons (**Fig. 3** in the main text and **Supplementary Figs. 2 and 3** online). High resolution images of stereocilia bundles in cochlear hair cells (**Fig. 2** in the main text and **Supplementary Fig. 1** online) were

recorded with sharp pipettes, with resistances of  $\sim 400$  M $\Omega$  (range 300-500 M $\Omega$ ) and estimated inner diameter of 30 nm. The pipette inner diameters are estimated from the pipette resistance<sup>5</sup> using a half cone angle of 3°.

## Instruments

The hopping technique requires careful damping of mechanical vibrations that arise from the large, rapid vertical motions of the Z-piezo with the attached probe. Our prototype has the nanopipette moving in the Z-direction while the sample is mounted on a separate piezo system moving it in the X-Y plane (**Fig. A**). This separation of Z-piezo from the X-Y piezos is required to prevent mechanical interference. The circuit that drives the movement of the piezo along the Z-axis is then tuned to allow a non-oscillating step response as fast as 1 ms.

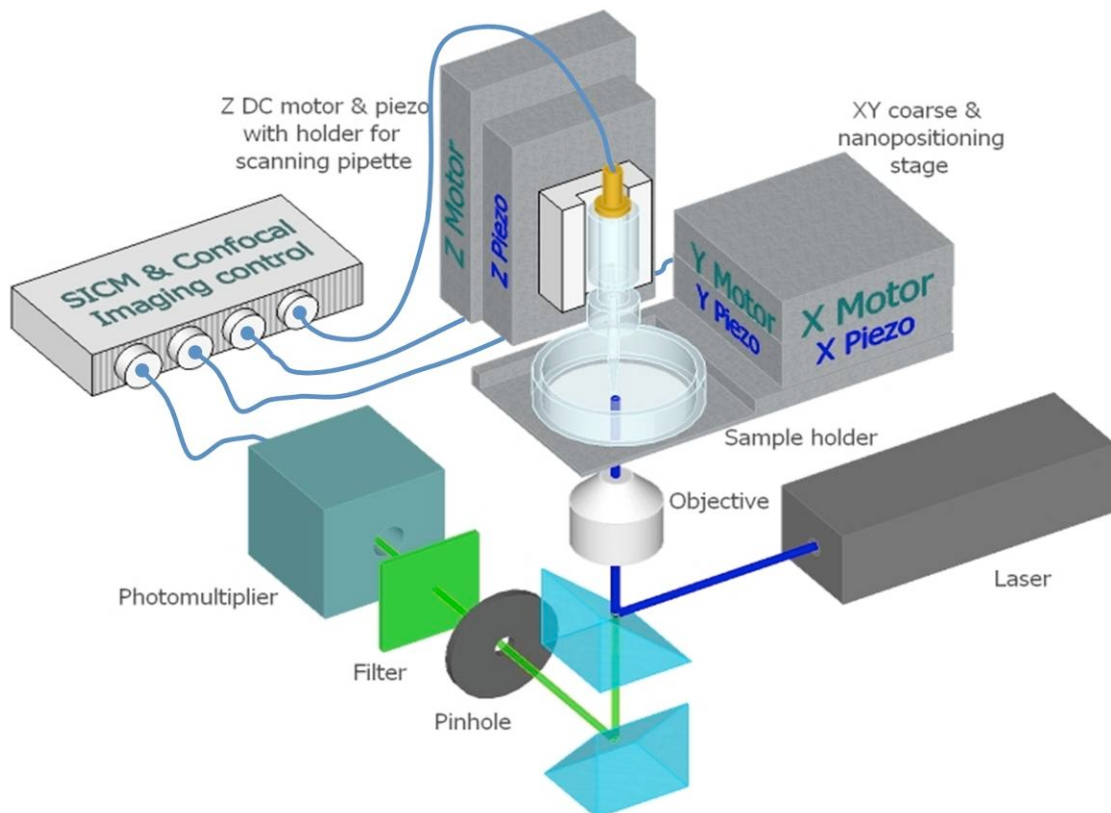


**Figure A.** A schematic of the hopping probe microscope, which is mounted on a stage of an inverted microscope and allows simultaneous topographic and fluorescence imaging.

All experiments were performed using a SICM scanner controller (Ionscope, UK) and scan head (Ionscope, UK). Two different heads were used for imaging (**Fig. A**). Scan head #1 consisted of a PIHera P-621.2 XY Nanopositioning Stage (Physik Instrumente (PI), Germany) with 100 x 100  $\mu\text{m}$  travel range that moved the sample and a LISA piezo actuator P-753.21C (PI, Germany) with travel range 25  $\mu\text{m}$  for pipette positioning along the Z-axis. Coarse positioning was achieved with translation stages M-111.2DG (XY directions) and M-112.1DG (Z-axis) (PI, Germany). The Z piezo actuator was driven by a 200 W peak power low voltage PZT amplifier E-505 (PI, Germany), while the XY nanopositioning stage was driven by 3 x 14 W amplifier E-503 (PI, Germany). Scan head #2 consisted of a P-733.2DD Ultra-High-Speed, XY Scanning Microscopy Stage (PI, Germany) customized for 10 x 10  $\mu\text{m}$  travel range (XY movement of the sample) and a LISA piezo actuator P-753.21C customized for 5  $\mu\text{m}$  travel range (PI, Germany) that moved the nanopipette along Z-axis. A translation stage M-112.1DG with a travel range of 25 mm (PI, Germany) was used for coarse positioning of the pipette in the Z-axis. All piezos were driven by 200 W peak power low voltage PZT amplifiers E-505 (PI, Germany). Scan head #2 was used for high resolution scanning of the cochlear hair bundles shown in **Figure 2f** in the main text. All other experiments were performed using scan head #1.

All piezo elements in both scan heads operated in capacitive sensor-controlled closed-loop using Sensor & Position Servo-Control Module E-509 (PI, Germany). Scan heads were placed on the platform of inverted Nikon TE200 microscope (Nikon Corporation, Japan). The pipette current was detected via an Axopatch 200B (Molecular Devices, USA) using a gain of 1 mV/pA and a low-pass filter setting of 5 kHz. The internal holding voltage source of the Axopatch-200B was used to supply a DC voltage of +200 mV to the pipette. The outputs of the capacitive sensors from all three piezo elements were monitored using Axon Digidata 1322A (Molecular Devices, USA) and Clampex 9.2 (Molecular Devices, USA).

The LCS-DTL-364 laser diode (473 nm wavelength, Laser Compact, Moscow, Russia) was used to provide the excitation light source during confocal microscopy measurements. The fluorescence signal was collected using oil-immersion objective 100x 1.3 NA, an epifluorescent filter block and a photomultiplier with a pinhole (D-104-814, Photon Technology International, Surbiton, England).

### Hopping mode protocol

The vertical Z positioning of the hopping probe and the movement of the sample in the XY plane were controlled by a SICM controller (Ionscope, UK) utilising a SBC6711 DSP board (Innovative Integration, USA) at a sampling frequency of 20 kHz. A three-step procedure was used to determine the height of the specimen at each imaging point. First, the probe was withdrawn from its existing position either by a specified distance or to a specified absolute height level. Second, the vertical position of the probe was maintained for 10 ms, while the nanopositioning stage moved the specimen to a new imaging point in the XY plane. During this time a reference current  $I_{REF}$  was measured as an average of the DC current through the HPICM probe. Finally, the probe was lowered at constant fall rate of 100 nm/ms (for a standard pipette) or 30 nm/ms (for a sharp pipette) while monitoring the difference in current,  $I$ , between  $I_{REF}$  and the instantaneous value of current through the probe  $I_{MV}$ . As soon as  $I$  exceeded the specified value of the setpoint,  $I_s$ , during at least four consecutive sample periods (that is 200  $\mu\text{s}$ ), the vertical position of the probe was saved

into the corresponding image pixel and the probe was quickly withdrawn by a specified hop amplitude to start a new measurement cycle.  $I_s$  values ranged from 0.25 to 1% of  $I_{REF}$ . See section “Approach curves” for details on the precision of the current measurements and vertical resolution.

During adaptive imaging (**Fig. 1e,f** in the main text), the final topography of a “512 x 512” pixels image was actually acquired in squares of different sampling/resolution depending on the roughness of each square. The sizes of the squares were 4 x 4, 8 x 8, 16 x 16, and 32 x 32 pixels, while the resolution levels were equivalent to 512 x 512, 256 x 256, 128 x 128, 64 x 64, 32 x 32, 16 x 16 pixels per whole image.

One or two different resolution levels were used. In each square, a quick pre-scan at 4 corner points (**Fig 1e** in the main text, low resolution prescan) was performed using specified hop amplitude of 3 to 6  $\mu\text{m}$  to determine the roughness,  $R_{PP}$ , and highest point  $H_{max}$ . Each square was then re-scanned at a higher resolution level if the estimated  $R_{PP}$  exceeded the user defined roughness threshold,  $R_T$ , otherwise the lower resolution level was used. In some cases, we simply imaged all squares with the same level of resolution either to produce a fast preview image (at a low resolution) or to ensure that no details were lost during adaptive scanning (a high resolution control).

High resolution images of the large areas of hippocampal neural network (e.g. **Fig. 3a** in the main text) were typically taken with a pre-scan hop amplitude of 5  $\mu\text{m}$ , square size of 4 x 4 pixels, two resolution levels of 256 x 256 and 128 x 128 pixels and  $R_T$  value of 100 nm. The pre-scan hop amplitude was reduced to 3  $\mu\text{m}$  and the  $R_T$  value to 25 nm for the high resolution scans of hair bundles (e.g. **Fig. 2b,c,e** in the main text). For medium resolution imaging of dendritic networks (e.g. **Fig. 3b,c** in the main text) the square size was typically increased to 8 x 8 pixels and the resolution levels of 128 x 128 and 64 x 64 were used. The overall time required to image the specimen varied significantly depending on the proportion of the sample area exhibiting high roughness. Generally speaking, the imaging time increases with slower probe fall rates (i.e. with sharper probes), smaller size of scan squares, higher pre-scan hop amplitude, and higher resolution level. High resolution images of elaborate samples (such as on **Fig. 3a** or **Fig. 2c** in the main text) took between 30 and 40 min. The images of less elaborated areas (such as in **Fig. 3b,c** or **Fig. 2f** in the main text) took 5 to 12 min. Note that at each imaging square the upward hopping typically starts at a different initial height. Therefore, the algorithm allows to “climb” up a tall sample without an excessive increase of the amplitude of the hops in each imaging square.

### Fluorescence measurement

After being kept for 15 min in the dark, dishes with hippocampal neurons were placed onto the XY nanopositioning stage in the scan head. Using an 10x objective and X, Y and Z translation stages for coarse movement, the HPICM pipette was positioned over the region of interest and lowered down to a safe distance of about 200  $\mu\text{m}$  from the sample surface. Then the 100x oil-immersion objective was chosen and an automated approach algorithm brought the HPICM probe to a distance of about one pipette radius from the sample surface. The XY position of the whole microscope platform was then adjusted to align the tip of the pipette with the confocal laser beam. To minimise photo-bleaching, fluorescence images of the selected area were recorded within 3 min separately from topography. The HPICM probe was retracted by ~24  $\mu\text{m}$  to prevent pipette – sample collisions during rapid

fluorescence acquisition. Topography imaging of the same area was performed immediately after obtaining a fluorescent image.

### Scanning Electron Microscopy

The fixed organs of Corti were dissected in ultra-pure distilled water, dehydrated in a graded series of acetone, and critical-point dried from liquid CO<sub>2</sub>. Then, the specimens were sputter-coated (EMS 575X Sputter Coater, Electron Microscopy Sciences, USA) with 5.0 nm of platinum under control with a film thickness monitor (EMS 150). The coated specimens were observed with a field-emission SEM (S-4800, Hitachi Technologies, Japan) at low accelerating voltage (1-5 kV).

### Image processing

Raw topography data obtained with varying resolution were interpolated using bilinear interpolation to produce a final image of 512 x 512 pixels. When required, the images were corrected to remove stripes caused by small displacement of XY nanopositioning stages in Z-axis and further corrected for the slope present in the preparations to aid visualisation of fine details.

### Approach curves

The experimental approach curve (**Fig. B**) demonstrates that the minimum reliably detectable current drop, expressed as a percentage of the reference current recorded far from surface ( $I_{REF}$ ), ranges from 0.25% (for a standard pipette of 100 nm inner diameter) to 0.75% (for a sharp pipette of 30 nm inner diameter). Because of the high signal-to-noise ratio of the current measurements in our experimental setup, the estimated vertical resolution at a 1% setpoint is 9 nm for a standard pipette and 6 nm for a sharp pipette. The real vertical resolution depends on the lateral dimension of the feature. The vertical sensitivity of the 30 nm pipette can be further improved to ~3 nm using a 1 kHz low-pass filter instead of a standard 5 kHz (**Fig. B**). However, this would reduce the response time of the feedback control.

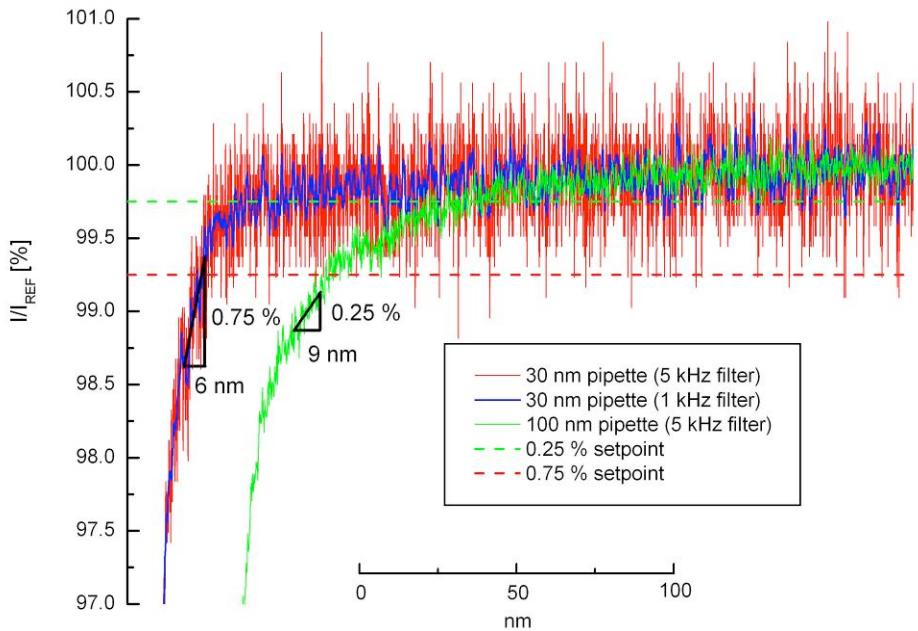


**Figure B.** Experimental approach curves. The green and red solid lines are the actual recordings of the current through the pipettes with 100 nm and 30 nm inner diameters respectively during the approach to a flat surface of a glass coverslip. Recordings were made using 5 kHz low-pass filter and the setup described above. The signal-to-noise ratio of the 30 nm pipette can be potentially improved two times by using a 1 kHz low-pass filter (blue solid line). Approach curves were normalized to a reference current recorded far from the surface ( $I_{REF} = 437$  pA for 30 nm pipette,  $I_{REF} = 1500$  pA for 100 nm pipette) and shifted horizontally relative to each other for clarity. Assuming that reliable detection of a non-stochastic change of the current occurs at a signal-to-noise ratio of 3:1, the minimum detectable current drops are indicated by green (100 nm pipette) and red (30 nm pipette) dashed lines. The corresponding minimum reliable setpoints are: 0.25% for 100 nm pipette and 0.75% for 30 nm pipette. The estimated vertical sensitivity at, a 1% setpoint is indicated for each pipette by black triangles together with the theoretical vertical resolution (6 nm for a 30 nm pipette and 9 nm for a 100 nm pipette).

### Long term stability

The drift of the pipette current is usually slow, initially with the rate of not more than 5% per 15 – 30 minutes and gradually slowing down below 5% per hour within the time span of couple of hours. Because the reference current and hence the setpoint ( $I_{REF}$  and  $I_S$ ) are corrected on every hop (i.e. about every 10 – 100 milliseconds), this drift never affects imaging. For example, during imaging of neurons (Fig. 3) and hair cells (Fig. 2) the current has decreased from 1870 pA to 1800 pA in 25 min and increased from 540 pA to 550 pA in 30 min, respectively.

## Spatial and temporal resolution

In this work we have used a borosilicate nanopipette with an inner diameter of about 30 nm and demonstrated a resolution of at least 16 nm by imaging stereocilia links (**Fig. 2f** in the main text). This is in accord with a prior SICM study where the resolution was estimated to be a fraction of the inner diameter of the probe<sup>6</sup>. We also reported previously a lateral resolution of 3-6 nm that was achieved with a 12.5 nm inner diameter SICM quartz probe<sup>7</sup>. It is not surprising, because the inner diameter of the nanopipette determines only the size of a “spherical sensing region”, while the actual lateral resolution is determined by the radius at the cross-section of this “spherical sensor” with the surface<sup>8</sup>. In principle, the highest lateral resolution should be achieved when the set-point is chosen in such a way that the distance between the pipette and the sample is just less than or equal to one pipette radius. In this case the diameter of this cross-section is small, which provides a resolution greater than the pipette inner radius, as found in this work. Here we directly compared the images of hair cells using HPICM and SEM and demonstrated a resolution better than 20 nm with a probe of 30 nm inner diameter. A similar data were obtained in live cells, where we have demonstrated that we can observe axons less than 50 nm, using hopping mode and the pipettes with an inner diameter of 100 nm (**Fig. 3** in the main text).

In addition to limitations imposed by the pipette size and the sample-to-probe distance, the resolution of our technique may also be limited by the resistance of the nanopipette. Extremely large resistances ( $> 2 \text{ G}\Omega$ ) will reduce the signal-to-noise ratio of current recordings and may slow down the imaging to a point where it becomes impractical. However, this is minimised in HPICM because we use the whole current passing through the pipette rather than a small fraction of this current as traditionally used in the “AC” modulation mode of SICM<sup>8</sup>. Even a very small pipette, with an inner diameter of 12.5 nm and the resistance of  $\sim 1 \text{ G}\Omega$ , passes an ion current of 200 pA at 200 mV, which results in reliable detection of the probe’s approach to the surface. Therefore, it is likely that even smaller pipettes could be used and lateral resolution below 10 nm should then be possible.

The speed of imaging is determined by the size of the image and the number of pixels required as well as by the total height and complexity of the sample. Adaptive scanning means that we can now scan only the pixels of interest, providing a significant improvement in imaging time. In HPICM, the time that is spent imaging each pixel is limited by the time taken to move the piezo vertically, which is currently limited by the resonance of the piezo to about 1 ms. The piezo resonances also impose a similar, albeit less important constraint on X-Y movements. However, these limitations could be minimised by shaping the voltage applied to the piezo to compensate for the resonance, or by designing the piezos with higher resonance frequencies, as has been done for high speed AFM<sup>9</sup>. In this work we have used a criterion of surface roughness for adaptive scanning to determine the number of pixels imaged in each square on the surface, reducing the effective resolution in squares where there are no features of interest. However other criteria could be used depending on the biological question of interest. For instance, the presence of a fluorescence signal could be used as the criterion to increase imaging resolution. Importantly, adaptive scanning allows us to obtain a low-resolution image of the sample in 1-2 min and then determine which regions to scan at higher resolution. This is analogous to an optical microscope where a low magnification is used to determine the area of interest before high resolution imaging.

## References

- Stepanyan, R., Belyantseva, I. A., Griffith, A. J., Friedman, T. B. & Frolenkov, G. I. *J. Physiol* **576**, 801-808 (2006).
- Shah, M. & Haylett, D. G. *J. Neurophysiol.* **83**, 2554-2561 (2000).
- Pyle, J. L., Kavalali, E. T., Choi, S. & Tsien, R. W. *Neuron* **24**, 803-808 (1999).
- Betz, W. J., Mao, F. & Bewick, G. S. *J. Neurosci.* **12**, 363-375 (1992).
- Ying, L., Bruckbauer, A., Rothery, A. M., Korchev, Y. E. & Klenerman, D. *Anal. Chem.* **74**, 1380-1385 (2002).
- Hansma, P. K., Drake, B., Marti, O., Gould, S. A. & Prater, C. B. *Science* **243**, 641-643 (1989).
- Shevchuk, A. I. *et al. Angew. Chem. Int. Ed Engl.* **45**, 2212-2216 (2006).
- Korchev, Y. E., Bashford, C. L., Milovanovic, M., Vodyanoy, I. & Lab, M. J. *Biophys. J.* **73**, 653-658 (1997).
- Ando, T. *et al. Proc. Natl. Acad. Sci. U. S. A* **98**, 12468-12472 (2001).